Self-Consistent Field Model of Polymer Adsorption: Generalized Formulation and Ground-State Solution

Harry J. Ploehn and William B. Russel*

Department of Chemical Engineering, Princeton University, Princeton, New Jersey 08544

Carol K. Hall

Department of Chemical Engineering, North Carolina State University, Raleigh, North Carolina 27695. *Received June 25, 1987*

ABSTRACT: In this work we formulate a general self-consistent field model of polymer adsorption and consider the case of nonionic homopolymer adsorption on a single, planar surface. Our approach is closely related to those of Edwards, Freed, and de Gennes in that we obtain a diffusion equation for the configuration probability of an idealized chain of polymer segments. Diffusion of configuration probability is driven by a potential field that depends upon the configuration of polymer segments and solvent molecules relative to the adsorbing surface; the statistical mechanical analysis of Helfand shows this field to be truly "self-consistent". Adsorption of segments by a "sticky" surface is featured in a new surface boundary condition. We solve the general field equation through an eigenfunction expansion, keeping only the first, or ground state, function in the expansion. The ground-state solution provides a variety of results, including adsorbed amount, bound fraction, surface volume fraction, root-mean-square layer thickness, and hydrodynamic thickness. Comparison with experimental data and the results of the Scheutjens–Fleer lattice model demonstrate that the present solution precludes the prediction of long, dangling tail configurations that influence many of the interactions of the adsorbed layer. However, the ground-state model accurately describes adsorbed layer characteristics near the surface. This approach is computationally more efficient and provides clearer physical insight than earlier models, motivating the development of better solutions of the general self-consistent field equations.

Introduction

Polymer adsorption plays a critical role in many technologically important processes, including adhesion, corrosion control, detergency, lubrication, drag reduction, film deposition, and membrane separations. Another common application of polymer adsorption is to control the stability of colloidal suspensions. Polymeric stabilization of dispersions (e.g., in paints, inks, pharmaceuticals, and foodstuffs) has received considerable attention,[1] but aggregation and flocculation processes are equally important and deserve examination. A good example of such a destabilization process is wastewater treatment. Polymeric flocculants are now an essential part of sludge processing operations such as thickening (increasing the solids concentration of an aqueous suspension) and dewatering (water removal from a suspension to form a slurry or cake). The selection of an effective polymeric flocculant, based on the polymer's chemistry and structure, and the determination of the proper dosage, mixing, and handling requirements are relevant practical problems that have been addressed largely on an empirical basis. The *design* of polymeric flocculants for particular systems and the *optimal* use of the flocculant require a theoretical understanding of polymer adsorption, interactions between adsorbed polymer layers, and the effect of these interactions on dispersion stability.

The stability of any colloidal suspension can be expressed through kinetic and thermodynamic criteria. The state of the suspension vis-à-vis these criteria depends on the interactions between suspended particles on a microscopic or molecular scale. For particles covered with layers of adsorbing polymer molecules, the range and strength of the interparticle interactions depend strongly upon the configuration of the adsorbed molecules. The polymer's configurational complexity gives rise to interesting interfacial properties but leads to considerable theoretical and computational difficulty. Although prediction of colloidal stability (or prediction of the interfacial properties of any polymer-modified system) is the ultimate goal, the fundamental problem is the analysis of the structure of adsorbed polymer layers.

The theoretical modeling of polymer adsorption has a long history and has been the subject of many reviews.[2] Early efforts treated an isolated polymer molecule near an adsorbing surface via statistical mechanical analyses of random walks near the surface, both on a lattice[3] and in continuous space.[4] These theories provide a description of the configuration of adsorbed molecules which includes the polymer–surface attraction and the entropic contribution of polymer configuration statistics but does not include "excluded-volume" interactions that derive from the free energy of mixing polymer and solvent. Later theories[5] incorporate excluded-volume interactions within a quasi-crystalline lattice model allowing calculation of site–site interactions through a mean-field approximation. Monte Carlo simulations[6] provide independent and mathematically exact results (such as adsorbed layer thickness and fractional coverage of the surface) for comparison with both the predictions of statistical mechanical theories and with experimental observations. Extension of the theoretical work to adsoption of multiple molecules has culminated in the development of several lattice models,[7] most recently that of Scheutjens and Fleer.[8]

The Scheutjens and Fleer (SF) lattice model describes many aspects of polymer adsorption. Space is discretized into layers of lattice sites parallel to a planar surface. The polymer molecule is modeled as a discrete "chain" of "segments" equal in size to the solvent molecules. Thus every lattice site contains either a segment or a solvent molecule. Site exclusion (repulsion) between segments is mediated by an attraction (characterized by the Flory–Huggins parameter χ) between segments and solvent molecules occupying neighboring sites. Use of the random mixing approximation within each layer represents a mean-field attempt to account for the interactions of segments well-separated along the contour of the chain but in close spatial proximity. Segments in the first layer contact the surface and receive an additional energy increment of χ_s (in units of kT) which characterizes the adsorption strength of segments relative to solvent molecules. The number of segments per chain, n, and the polymer volume fraction in bulk solution, φ_b, complete the description.

The SF model succeeds for several reasons. First, the model treats a wide range of experimental conditions without a priori assumptions about the configuration of

0024-9297/88/2221-1075$01.50/0

the polymer molecules in the adsorbed layer. Also, the statistical distributions of trains, loops, and tails are enumerated, highlighting the influence of particular configurations, especially tails, on experimentally observable quantities. The results indicate a relative surplus of chain ends far from the surface, while the region near the surface is depleted of chain ends. This conclusion agrees with earlier results[9] which predict that adsorbed chains prefer long tail/short loop configurations rather than short tail/long loop configurations. These "end effects" have a significant effect on hydrodynamic layer thicknesses[10,25] and forces between interacting adsorbed polymer layers.[11]

On the other hand, the SF model is limited in several respects. The model equations are written in a finite difference form that facilitates numerical solution but obscures much of the underlying physics. The discretization of space, necessitating the selection of a particular lattice geometry, is an artificial approximation that may not accurately reflect the reality of continuous space. The consequences may be most serious near the surface, where important details of the segment–surface interaction occur on a length scale comparable to the spacing between lattice layers. On a more practical level, the lattice model calculations become time consuming for long chains or for the construction of colloidal phase diagrams.

We have addressed these limitations through the self-consistent field approach, originally developed by Edwards[12] for the study of polymer solutions. The idea was extended to adsorbing polymer by DiMarzio[3] and de Gennes,[13] with practical implementation for near-Θ solvents by Jones and Richmond.[14] This method relies on the fact that the statistics of polymer random walks are described by a diffusion equation.[9] Indeed, there is a strong analogy between the contour of a polymer molecule embedded in an adsorbed polymer matrix and the trajectory of a diffusing particle in an external potential field. Formulation of the problem as a field equation brings to bear a variety of solution techniques and permits extensions to important related problems.

In this work we formulate a general self-consistent field (SCF) model for polymer adsorption and consider the case of nonionic homopolymer adsorption at a single, planar surface. The model takes the form of the familiar diffusion equation for the probability of chain configurations, developed by Chandrasekhar[9] and employed by many others.[3-8,12-15,17,18,23,29] We incorporate a self-consistent potential field (which drives the diffusion equation) developed from the statistical mechanical analyses of Helfand[18] or Dickman and Hall.[19] The polymer–surface interaction, modeled as a "sticky surface" attraction, produces a new surface boundary condition for the diffusion equation. We solve the SCF equations through a ground-state approximation[14,15] which yields an analytical expression for the volume fraction profile of polymer segments near the surface. Other features, including the total adsorbed amount of polymer, the fraction of segments in contact with the surface, the root-mean-square layer thickness, and the hydrodynamic thickness, are calculated from the volume fraction profile and are compared with experimental results. Such comparisons motivate the development of more sophisticated models of this type.

Theory

A. Self-Consistent Field Equation. The structural complexity of linear polymer molecules necessitates a statistical description of molecular configurations. Analyses of the configurational statistics of polymers have been presented in several comprehensive works,[12,15,17,18] wherein the goal is to relate the system's physical characteristics to unambiguous mathematical expressions. Instead of considering the detailed configuration of the bonds in a real polymer molecule, we employ the usual abstraction of the molecule as a "chain" of statistical "segments" with the number of bonds per segment chosen so that the chain exhibits random-flight statistics. A polymer configuration is described by the set of spatial positions of each segment of the chain, analogous to the position in space of a diffusing particle at successive, discrete times. The sequence of segments corresponds to a particle trajectory, with the rank of a segment (position in the chain relative to one end) replacing time. Such a function of a random variable (spatial position) and time (segment rank) defines a stochastic process.

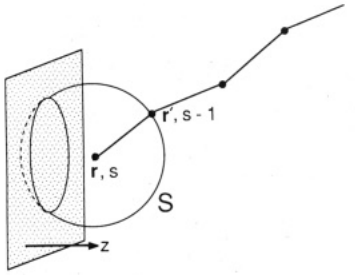

Figure 1. For positions **r** such that $z \geq l$, S is a spherical locus of segment positions **r'** that contribute to the integral in eq 1. When $z < l$, the spherical locus is truncated by the adsorbing surface, producing the spatial anisotropy manifested in eq 14b and 15.

A stochastic process consists of a hierarchy of probability densities which are governed by consistency conditions found in standard texts.[16] Such a description is complete but cumbersome and must be simplified through additional assumptions. One assumption, alluded to already, is that a chain of segments exhibits random-walk statistics: traveling down the contour of the chain, a segment's position depends only on the position of the previous segment. This type of stochastic process is known as a Markov process.

In reality, the distribution of chain configurations depends not only on the connectivity of the chains but also upon their interactions which may be conveniently expressed in terms of a potential field acting on the segments of the chains. The potential acting upon an individual segment depends on the distribution of all other segments in the system, which is at least known in probabalistic terms.[17] Within the spirit of the present theory, we assume that the configuration-dependent potential may be redefined by averaging over the segment distribution, yielding a "potential of mean force". This mean-field approximation decouples the many-body problem[17] and makes the present field equation formulation possible. We postpone briefly the discussion of the form of the potential that makes the calculation "self-consistent".

A field equation describing the configurations of adsorbed chains may be derived from first principles, namely, the consistency conditions defining a stochastic process.[41] A heuristic description, though, provides a complete yet concise exposition. Suppose that $G(\mathbf{r},s)$ is the (unnormalized) probability density of a chain of contour length s that ends within $d\mathbf{r}$ of spatial position **r**. Recognizing that G is governed by a Markov process, we can express G as the integral of the product of two other probability densities. The first, $G(\mathbf{r}',s-l)$, is the probability density of a chain of contour length $s - l$ that ends within $d\mathbf{r}'$ of a spatial position **r'** which itself lies a segment length l away from position **r** (see Figure 1, ignoring the plane, for now). The second factor, $e^{-\beta U(\mathbf{r})}$, is the probability density

for placing a single segment at $\mathbf{r}$; U is the potential field acting on the segment. This product, integrated over all possible positions of $\mathbf{r}'$ (denoted by the locus S) gives an equation for G, specifically

$$G(\mathbf{r},s) = \frac{e^{-\beta U(\mathbf{r})}}{4\pi l^2}\int_S G(\mathbf{r}',s-l)\,dS \tag{1}$$

where $4\pi l^2$ normalizes the integral. Expanding $G(\mathbf{r}',s-l)$ in a Taylor series in $\mathbf{r}$ and s, integrating, and rearranging produce the self-consistent field (SCF) equation

$$l\frac{\partial G}{\partial s} = \frac{l^2}{6}\nabla^2 G + [1 - e^{\beta U(\mathbf{r})}]G \tag{2}$$

with the initial condition

$$G(\mathbf{r},0;\mathbf{r}_s) = \delta(\mathbf{r} - \mathbf{r}_s) \tag{3}$$

ensuring that chains start at *some* position denoted by $\mathbf{r}_s$. Equation 2 is encountered in many theories of polymer adsorption[6-9,13-15,18,21,23,29] and is the basis for further analysis here.

B. Segment Volume Fraction Profile and Equilibrium Condition. Next, the configuration probability $G(\mathbf{r},s)$ must be related to physical quantities, such as the segment volume fraction $\varphi(\mathbf{r})$. To do so, we observe that every segment (at some contour location s) belonging to a chain of total length nl is, in fact, the junction of two "subchains" of length s and $nl - s$ (n is the number of segments per chain). The volume fraction is the probability of finding *any* segment, regardless of contour location, at a spatial position $\mathbf{r}$; thus $\varphi(\mathbf{r})$ is proportional to the probability that two subchains of combined length nl meet at position $\mathbf{r}$, integrated over all possible contour locations of the junction. Mathematically, the relation

$$\varphi(\mathbf{r}) = \frac{c}{e^{-\beta U(\mathbf{r})}}\int_0^{nl} G(\mathbf{r},s)G(\mathbf{r},nl-s)\,ds \tag{4}$$

represents this probability. The factor $e^{-\beta U(\mathbf{r})}$ arises naturally to remedy the double-counting of the junction segment in the product $G(\mathbf{r},s)G(\mathbf{r},nl-s)$, and c is a proportionality constant. Far from an adsorbing surface, chains have an equal probability of ending anywhere, and the polymer volume fraction goes to its bulk value; hence $G(\mathbf{r},s) \to 1$, $\varphi(\mathbf{r}) \to \varphi_b$, and, as will be developed below, $U(\mathbf{r}) \to 0$ far from the surface. Equation 4 then yields $c = \varphi_b/n$. In a sense, this procedure includes a chain configuration from the bulk solution in the partition function for the adsorbed layer and implies equilibrium between free and adsorbed chains. Alternately, a proper statistical mechanical calculation of the chemical potentials of adsorbed and free chains[18,41] leads to a formal equilibrium condition.

C. Self-Consistent Field. The field equation (2) is closed through the specification of a self-consistent field (SCF) $U(\mathbf{r})$ that depends upon the configuration of the adsorbed polymer molecules. Arbitrary specification of $U(\mathbf{r})$ *does not* guarantee that $G(\mathbf{r},s)$ is proportional to the number of chains of length s that end at $\mathbf{r}$. An equilibrium condition is needed to ensure that the chemical potentials of all chains in all configurations are equal, thus giving proper weight to each configuration.

Differentiating the free energy of the system (including chains and solvent molecules) with respect to the number of chains in an arbitrary configuration produces the chemical potential of that configuration; equating this quantity with the chemical potential of chains in bulk solution ensures that adsorbed chains are in equilibrium with each other as well as with those in bulk solution. Naturally the free energy of the system depends (through the partition function) upon the free energy of individual segments and solvent molecules as determined by their particular interactions; the latter relationship is provided by an appropriate polymer solution theory.

Scheutjens and Fleer[8] calculate the partition function, free energy, and the SCF for polymer chains and solvent on a lattice by using the Flory solution theory. An earlier and more general derivation by Helfand[18] can accommodate an arbitrary polymer solution/mixture theory and has been extended to interfacial systems of bulk polymer and copolymer blends.[21] Helfand's formulation is based on a continuous space model of polymer configurations. For an incompressible system, neglecting nonlocal interactions, Helfand finds

$$U(\mathbf{r}) = l^3\frac{\partial \Delta f^*}{\partial \varphi} \tag{5}$$

in which $\varphi(\mathbf{r})$ is the segment volume fraction. With $1 - \varphi(\mathbf{r})$ representing the solvent volume fraction, the free energy density $\Delta f^*(\varphi)$ of a solution relative to bulk solution (i.e., far from the surface) is

$$l^3\Delta f^* = l^3 f(\varphi) - \varphi\mu_p{}^b - (1-\varphi)\mu_s{}^b - \frac{kT\varphi}{n}\ln\frac{\varphi}{n} \tag{6}$$

where f is the free energy density of a homogeneous solution, $\mu_p{}^b$ and $\mu_s{}^b$ are the segment and solvent chemical potentials evaluated at bulk solution conditions, and n is the number of segments per chain.

In this work we employ the Flory polymer solution theory[22] which is suitable for a wide range of solvent conditions, although of questionable accuracy for calculations in continuous space.[19] The free energy density is

$$l^3 f(\varphi) = \varphi\mu^\circ{}_p + (1-\varphi)\mu^\circ{}_s + kT\left[(1-\varphi)\ln(1-\varphi) + \frac{\varphi}{n}\ln\frac{\varphi}{n} + \chi\varphi(1-\varphi)\right] \tag{7}$$

where $\mu^\circ{}_p$ and $\mu^\circ{}_s$ are the chemical potentials of bulk amorphous polymer (on a per segment basis) and pure solvent having the same molecular size as a polymer segment. Differentiation of f with respect to the *number* of segments and solvent molecules and evaluation at φ_b, the segment volume fraction in bulk solution, yield $\mu_p{}^b$ and $\mu_s{}^b$. From eq 6 and 7 Δf^* follows as

$$l^3\beta\Delta f^* = (1-\varphi)\ln\frac{(1-\varphi)}{(1-\varphi_b)} - \chi(\varphi-\varphi_b)^2 + \varphi - \varphi_b$$

with $\beta = 1/kT$, giving

$$\beta\frac{\partial \Delta f^*}{\partial \varphi} = \beta U(\mathbf{r}) = -\ln\frac{(1-\varphi)}{(1-\varphi_b)} - 2\chi(\varphi-\varphi_b) \tag{8}$$

as the resultant SCF, which, incidentally, is in complete agreement with the results of the lattice-based calculations of Scheutjens and Fleer.[8]

Equation 8 may also be found through the theory of Dickman and Hall,[19] who seek an accurate equation of state for homogeneous polymer solutions through a continuous space model. After defining the partition function for a system of many chains, they develop an "osmotic equation of state" which relates the osmotic pressure of the system to the probability of inserting a "test" chain into the system. Inversion of the equation of state for single segments gives the segment "insertion probability" as a function of osmotic pressure. Substitution of the osmotic pressure given by the Flory theory into the inverted equation produces eq 8.

The SCF should also account for the inpenetrability of the surface as well as its adsorptive strength. For a planar

adsorbing surface at $z = 0$, the SCF is assumed to be infinite for $z < 0$ so that adsorption takes place in the half-space $z \geq 0$. The form of the interactions between the surface and the segments and solvent is a more delicate matter. Although the true interaction is probably either van der Waals attraction or hydrogen bonding, the necessary physical parameters are not known. Instead, we utilize a square well adsorption potential similar to that used by Baxter[20] for suspensions of hard spheres with adhesion. With χ_s as the adsorption energy (in units of kT) of segments relative to solvent, we write

$$\begin{aligned} \beta U_{ads} &= 0 \qquad z > \epsilon \\ &= -\chi_s + \ln(\epsilon/l) \qquad z < \epsilon \end{aligned} \tag{9}$$

as the adsorption strength. Calculating the exponential of both sides and taking the limit as $\epsilon \to 0$ produce

$$e^{-\beta U_{ads}} = \delta(z)e^{\chi}s \tag{10}$$

which is appropriate when the range of the true adsorption potential is small compared to the segment length. Although the probability density $e^{-\beta U_{ads}}$ is discontinuous and diverges at $z = 0$, the integrated probability of adsorption remains finite. Combining the contributions of adsorption and segment–solvent mixing,

$$\begin{aligned} \beta U &= \infty \qquad z < 0 \\ &= -\ln[\delta(z)e^{\chi}s] - \ln\frac{(1-\varphi)}{(1-\varphi_b)} - 2\chi(\varphi - \varphi_b) \qquad z \geq 0 \end{aligned} \tag{11}$$

represents the total SCF.

D. Surface Boundary Condition. Equation 11 implies that $e^{-\beta U(\mathbf{r})}$ as well as $G(\mathbf{r},s)$ are discontinuous at $z = 0$. Obviously, the Taylor series expansion of $G(\mathbf{r}',s-l)$ fails at this point, so the probability density G must be written as the sum of a continuous part, G_c, and a surface function, G_s, through

$$G(\mathbf{r},s) = G_c(\mathbf{r},s) + \delta(z)G_s(s) \tag{12}$$

Substitution into (1) gives

$$G_c(\mathbf{r},s) + \delta(z)G_s(s) = \frac{e^{-\beta U(\mathbf{r})}}{4\pi l^2}\int_S [G_c(\mathbf{r}',s-l) + \delta(z')G_s(s-l)]\,dS \tag{13}$$

where the integration is over the locus of positions $\mathbf{r}'$ which are a segment length from $\mathbf{r}$. As before, $G_c(\mathbf{r}',s-l)$ is expanded in $\mathbf{r}$ and s, while $G_s(s-l)$ is expanded in s. For positions $\mathbf{r}$ such that $z \geq l$, integration yields the same SCF eauation (2) as found earlier. However, when $z < l$, the spherical locus of neighbors, truncated by the surface (see Figure 1), produces a SCF equation for the anisotropic surface region

$$G_c(\mathbf{r},s) + \delta(z)G_s(s) = e^{-\beta U(\mathbf{r})}K(z,G_c,G_s) \qquad 0 < z < l \tag{14a}$$

with

$$K(z,G_c,G_s) = \mathbf{D}:\nabla\nabla G_c + \left[\frac{1}{2}\left(1+\frac{z}{l}\right) + \frac{l}{4}\left(1-\frac{z^2}{l^2}\right)\times \mathbf{k}\cdot\nabla\right]\left(G_c - l\frac{\partial G_c}{\partial s}\right) + \frac{1}{2}\left[1-\frac{z^2}{l^2}\right]^{1/2}\left(G_s - l\frac{\partial G_s}{\partial s}\right) \tag{14b}$$

Here $\mathbf{k}$ is the unit normal to the surface and

$$\mathbf{D} = \frac{1}{24l}[[z(3l^2 - z^2) + 2l^3][\mathbf{ii} + \mathbf{jj}] + 2(l^3 + z^3)\mathbf{kk}] \tag{15}$$

is a tensor that reduces to $(l^2/6)\,\mathbf{I}$ at $z = l$. The product $e^{-\beta U(\mathbf{r})}K(z,G_c,G_s)$ is just the probability that a chain of length s reaches $\mathbf{r}$. The first term in $K(z,G_c,G_s)$, eq 14b, is the contribution from the random walk of the chain with the spatial anisotropy of the surface region reflected in the z-dependence of $\mathbf{D}$. The spatial anisotropy is also responsible for the gradient appearing in the second term. Finally, the third term represents a source of *extra* probability arising from the "surface phase" of adsorbed segments not accounted for in G_c.

A surface boundary condition is derived by integrating eq 14 over a differential interval near the surface. The result,

$$G_s(s) = e^{-\beta U_s}K(0,G_c,G_s) \tag{16}$$

depends on the surface SCF

$$\beta U_s \equiv -\chi_s - \ln\frac{(1-\varphi)}{(1-\varphi_b)} - 2\chi(\varphi - \varphi_b) \tag{17}$$

from eq 11 defined at $z = 0$. Let U_c be the continuous part of the SCF so that for $z > 0$ and in the limit $z \to 0$, $U_c \equiv U$. Thus, from eq 14a,

$$G_c(\mathbf{r},s) = e^{-\beta U_c}K(z,G_c,G_s)$$

for $z > 0$. Taking the limit $z \to 0$ and combining with (16) give

$$G_s(s) = K_A G_c(\mathbf{r}_0,s) \tag{18}$$

where $\mathbf{r}_0 = (x,y,0)$ and

$$K_A \equiv e^{-\beta[U_s - U_c(\mathbf{r}_0)]} \tag{19}$$

defines a partition coefficient for segments on or near the surface. Substitution of eq 18 into 14 produces the SCF equation

$$G_c(\mathbf{r},s)e^{\beta U_c} = \mathbf{D}:\nabla\nabla G_c + \left[\frac{1}{2}\left(1+\frac{z}{l}\right) + \frac{l}{4}\left(1-\frac{z^2}{l^2}\right)\mathbf{k}\cdot\nabla\right]\times \left(G_c - l\frac{\partial G_c}{\partial s}\right) + \frac{1}{2}K_A\left[1-\frac{z^2}{l^2}\right]^{1/2}\times \left[G_c(\mathbf{r}_0,s) - l\frac{\partial G_c}{\partial s}(\mathbf{r}_0,s)\right] \tag{20}$$

valid in the surface region $z < l$. At $z = 0$, neglecting the $\nabla\nabla G_c$ term and the cross derivative $\nabla(\partial G_c/\partial s)$ relative to the ∇G_c term in $K(0,G_c,G_s)$ leaves

$$G_c(\mathbf{r}_0,s)e^{\beta U_c(\mathbf{r}_0)} = \frac{1}{2}(K_A + 1)\left[G_c - l\frac{\partial G_c}{\partial s}\right] + \frac{l}{4}\mathbf{k}\cdot\nabla G_c \qquad z = 0 \tag{21}$$

as the surface boundary condition.

The segment volume fraction is also discontinuous at the surface. Using the relation

$$e^{-\beta U} = e^{-\beta U_c}[1 + \delta(z)K_A] \tag{22}$$

substitution of eq 12 into 4 produces

$$\varphi(\mathbf{r}) = \frac{\varphi_b[1 + \delta(z)K_A]}{nle^{-\beta U_c(\mathbf{r})}}\int_0^{nl} G_c(\mathbf{r},s)G_c(\mathbf{r},nl-s)\,ds \tag{23}$$

Rewriting eq 23 in a more compact form,

$$\varphi(\mathbf{r}) = \varphi_c(\mathbf{r})[1 + \delta(z)K_A] = \varphi_c(\mathbf{r}) + \delta(z)\varphi_s \tag{24}$$

defines a continuous volume fraction profile $\varphi_c(\mathbf{r})$ as well as the "surface fraction"

$$\varphi_s(\mathbf{r}) = K_A\varphi_c(\mathbf{r}_0) \tag{25}$$

of segments actually on the surface.

E. Summary. The self-consistent field model of polymer adsorption consists of a complete, closed set of

equations developed herein. For a randomly adsorbing homopolymer, the variation of the adsorbed layer structure normal to the surface is more significant than variations parallel to the surface if there is sufficient overlap of adsorbed chains. This condition is usually met in practice when the chains are long enough so that significant adsorption occurs, even though the adsorption energy per segment may be small. We assume that chain configurations are evenly distributed over the surface and that the length scale of fluctuations about the equilibrium distribution is small compared to the average lateral dimension of an adsorbed chain.

Consequently, the segment volume fraction profile, the self-consistent field, and the configuration probability density vary only with z and s but not with lateral position or time. Making z and s dimensionless with l, the self-consistent field equations are

$$\frac{\partial G_c}{\partial s} = \frac{1}{6}\frac{\partial^2 G_c}{\partial z^2} + [1 - e^{\beta U_c}]G_c \qquad z \geq 1 \tag{26}$$

$$G_c e^{\beta U_c} = \frac{1}{12}(1 + z^3)\frac{\partial^2 G_c}{\partial z^2} + \left[\frac{1}{2}(1 + z) + \frac{1}{4}(1 - z^2)\frac{\partial}{\partial z}\right]\left(G_c - \frac{\partial G_c}{\partial s}\right) + \frac{1}{2}K_A[1 - z^2]^{1/2}\left[G_c(0,s) - \frac{\partial G_c}{\partial s}(0,s)\right] \qquad 0 < z < 1 \tag{27}$$

with boundary conditions and initial condition

$$G_c(0,s)e^{\beta U_c(0)} = \frac{1}{2}(K_A + 1)\left[G_c(0,s) - \frac{\partial G_c}{\partial s}(0,s)\right] + \frac{1}{4}\frac{\partial G_c}{\partial z}(0,s) \tag{28}$$

$$G_c(\infty,s) = 1 \tag{29}$$

$$[1 + \delta(z)K_A]G_c(z,0) = \delta(z - z_s) \tag{30}$$

with z_s as the arbitrary starting position, segment volume fraction profile

$$\varphi_c(z) = \frac{\varphi_b}{n e^{-\beta U_c(r)}}\int_0^n G_c(z,s)G_c(z,n-s)\,ds \tag{31a}$$

$$\varphi_s = K_A\varphi_c(0) \tag{31b}$$

with

$$K_A = e^{-\beta[U_s - U_c(0)]} \tag{32}$$

and self-consistent field

$$\beta U_c = -\ln\frac{(1 - \varphi_c)}{(1 - \varphi_b)} - 2\chi(\varphi_c - \varphi_b) \qquad z \geq 0 \tag{33a}$$

$$\beta U_s = -\chi_s - \ln\frac{(1 - \varphi_s)}{(1 - \varphi_b)} - 2\chi(\varphi_s - \varphi_b) \qquad z = 0 \tag{33b}$$

The four parameters which describe the chemistry of the system are n, φ_b, χ, and χ_s. This set of equations is amenable to solution by a variety of analytical and numerical techniques, each involving its own approximations.

Ground-State Solution

A. Segment Volume Fraction Profile. The self-consistent field equations (26) and (27), along with the accompanying conditions and definitions (28)–(33), are a closed, albeit nonlinear, system of equations which can, in principle, be solved exactly. Levine et al.[7] recognized the close relationship between these field equations and the recurrence relations of their lattice model. In fact, the Scheutjens–Fleer (SF) lattice model[8] is a finite difference analogue of the SCF equation (2) which is solved iteratively. For long chains, convergence is very slow and sensitive to the initial guess, resulting in very tedious calculations. Furthermore, the results are sensitive to the choice of lattice geometry.

In order to overcome these limitations, we obtain an analytical solution similar to those developed by de Gennes,[15] Jones and Richmond,[14] and Joanny et al.[23] These approaches rely on the "pseudolinearity" of the SCF equation if the SCF is regarded as an arbitrary external field. The probability density $G_c(z,s)$ is expanded in the eigenfunctions of the linear operator of the SCF equation so that

$$G_c(z,s) = \sum_k g_k(z)\exp(\lambda_k s) \tag{34}$$

where λ_k are the eigenvalues. If the chain has polymeric length, the $k = 0$ term dominates the higher order terms which are usually neglected.

We combine the higher order eigenfunctions into a composite function G' defined by

$$G_c(z,s) = g(z)\exp(\lambda_0 s) + G'(z,s) \tag{35}$$

where $g(z)$ and λ_0 are the ground-state eigenfunction and eigenvalue. This work addresses the ground-state solution for $g(z)$, leaving to a later time the solution of the higher order equations, so that G' is neglected. Recalling the initial condition (30), integration of (35) produces

$$\int_0^\infty [1 + \delta(z)K_A]g(z)\,dz = 1 \tag{36}$$

as a normalization condition for $g(z)$. Furthermore, we neglect the influence of the surface region governed by eq 27, assuming 26 to apply up to the surface $z = 0$. Substitution of eq 35 (neglecting G') into (26), (28), and (31a) produces the ground-state equation

$$\frac{1}{6}\frac{d^2 g}{dz^2} + [1 - \lambda_0 - e^{\beta U_c}]g = 0 \tag{37}$$

the surface boundary condition at $z = 0$

$$\frac{1}{4g(0)}\frac{dg(0)}{dz} = e^{\beta U_c(0)} - \frac{1}{2}(K_A + 1)(1 - \lambda_0) \tag{38}$$

and the volume fraction profile

$$\varphi_c(z) = \varphi_b e^{n\lambda_0}e^{\beta U_c}g^2(z) \tag{39}$$

Further analytical progress requires linearizing the Boltzmann factor

$$e^{\beta U_c} = \frac{1 - \varphi_b}{1 - \varphi_c}e^{-2\chi(\varphi_c - \varphi_b)} \tag{40a}$$

as

$$e^{\beta U_c} \approx \frac{1 - \varphi_b}{e^{-2\chi\varphi_b}}[1 + (1 - 2\chi)\varphi_c + (1 - 2\chi + 2\chi^2)\varphi_c^2] \tag{40b}$$

with φ_b assumed to be small so that $(1 - \varphi_b)e^{2\chi\varphi_b} \approx 1$. Alternately, eq 40b becomes

$$e^{\beta U_c} \approx 1 + \upsilon\varphi_c + \frac{w}{2}\varphi_c^2 \tag{41}$$

with $\upsilon = \xi(1 - 2\chi)$, $w = 2\xi^2(1 - 2\chi + 2\chi^2)$, and ξ as the fraction of the segment volume occupied by polymer, defined in eq 56. The linearization is a very good approximation at all but the highest segment volume fractions found near the surface. Consequently, the *exact* Boltzmann factor of eq 40a is used in the surface boundary condition. Usually the latter two terms of (41) may be neglected when compared with unity so that rearrangement of (39) yields

$$g(z) = (\varphi_c/K)^{1/2} \tag{42}$$

with $K = \varphi_b e^{n\lambda_0}$. Using (42) to eliminate $g(z)$ from (37) with $e^{\beta U_c}$ from (41) gives

$$\frac{d^2\varphi_c}{dz^2} - \left[\frac{d\varphi_c}{dz}\right]^2 \frac{1}{2\varphi_c} - 12\left[\lambda_0 + \upsilon\varphi_c + \frac{w}{2}\varphi_c^2\right]\varphi_c = 0 \tag{43}$$

while (38) becomes

$$\frac{1}{8\varphi_c(0)}\frac{d\varphi_c(0)}{dz} = e^{\beta U_c(0)} - \frac{1}{2}(K_A + 1)(1 - \lambda_0) \tag{44}$$

with $e^{\beta U_c(0)}$ given by (40a) evaluated at $z = 0$.

The first integral of (43) with boundary condition $\varphi_c \to \varphi_b \approx 0$ as $z \to \infty$ is

$$\left[\frac{d\varphi_c}{dz}\right]^2 = 24\varphi_c^2\left(\lambda_0 + \frac{\upsilon}{2}\varphi_c + \frac{w}{6}\varphi_c^2\right) = \left[-\varphi_c\left[24\left(\lambda_0 + \frac{\upsilon}{2}\varphi_c + \frac{w}{6}\varphi_c^2\right)\right]^{1/2}\right]^2 \tag{45}$$

with the negative root selected so that the profile decays with increasing z. Integrating a second time gives the volume fraction profile

$$\varphi_c(z) = \frac{4\lambda_0 c_i e^{\gamma z}}{\left(c_i e^{\gamma z} - \frac{\upsilon}{2}\right)^2 - \frac{2}{3}\gamma_0 w} = \frac{4\lambda_0 c_i e^{-\gamma z}}{\left(c_i - \frac{\upsilon}{2}e^{-\gamma z}\right)^2 - \frac{2}{3}\lambda_0 w e^{-2\gamma z}} \tag{46}$$

where $\gamma = (24\lambda_0)^{1/2}$ and c_i is an integration constant to be determined from the surface boundary condition (28) (in conjunction with eq 31b, 32, 33b, 40a, 45, and 46).

In practice, the undetermined constants λ_0 and c_i are found through an iterative solution of the nonlinear algebraic equations. The quantity $1/\lambda_0$ represents a characteristic chain length; for sections of chains longer than $1/\lambda_0$, the effects of adsorption and solvency cause the chain to deviate from the ideal random-walk state. Given n, φ_b, χ, and χ_s, λ_0 is guessed. Equations 31b, 32, 33b, 40a, and 45 are solved iteratively for $\varphi_c(0)$ and eq 46 then determines c_i. Finally, the normalization condition (36), rewritten using (42) as

$$1 = \frac{1}{(\varphi_b e^{n\lambda_0})^{1/2}}\int_0^\infty [1 + \delta(z)K_A](\varphi_c)^{1/2}\, dz \tag{47}$$

determines the accuracy of the guessed value of λ_0. A new value of λ_0 is selected, and the iteration is repeated until eq 47 is satisfied.

B. Adsorbed Layer Characteristics. The volume fraction profile, eq 46, contains considerable information for characterization of the layer of adsorbed polymer chains. Unfortunately, $\varphi_c(z)$ cannot be routinely measured, although a few profiles have been obtained through neutron scattering.[24,25] Characterization is presently based on calculated or measured quantities which represent weighted integrals of the volume fraction profile.

The first important adsorption characteristic is the total adsorbed amount of polymer, φ_{ads}. An analytical expression for φ_{ads},

$$\varphi_{ads} = K_A\varphi_c(0) + \frac{1}{2w^{1/2}}\ln\left\{\frac{c_i + \left[\frac{2}{3}\lambda_0 w\right]^{1/2} - \frac{\upsilon}{2}}{c_i - \left[\frac{2}{3}\lambda_0 w\right]^{1/2} - \frac{\upsilon}{2}}\right\} \tag{48}$$

found by integrating eq 46, includes the bound segments as the first term. The bound fraction

$$p = \varphi_s/\varphi_{ads} \tag{49}$$

is the fraction of segments that are actually adsorbed on the surface. Finally, the root-mean-square (RMS) layer thickness

$$t_{RMS} = \left[\frac{1}{\varphi_{ads}}\int_0^\infty z^2\varphi_c(z)\, dz\right]^{1/2} \tag{50}$$

is calculated numerically. The quantities φ_{ads}, p, and t_{RMS} may be measured experimentally by using a variety of techniques, including ellipsometry,[30-35] infrared,[36,37] NMR,[38] and ESR[39] spectroscopy.

Hydrodynamic techniques also measure a thickness of adsorbed layers. In the capillary method, the measured flux of solvent through a polymer-coated capillary is related to the apparent capillary radius; subtraction of the actual radius gives the hydrodynamic thickness of the adsorbed layer. Alternately, dynamic light scattering measures the apparent radius of polymer-coated particles suspended in a solvent; again, subtraction of the bare particle radius yields the hydrodynamic thickness.

Several groups, including Cohen Stuart et al.,[10] Varoqui and Dejardin,[26] and Anderson and Kim,[27] have developed models of solvent flow through adsorbed polymer layers. In our weak flow calculations, a shear flow of solvent is imposed on a stationary adsorbed layer. Assuming that the solvent flow is parallel to the surface, the solvent velocity $V(z)$ satisfies the dimensionless Debye–Brinkman equation

$$\frac{d^2V}{dz^2} - 18\eta f\varphi V = 0 \tag{51}$$

with $V = 0$ at $z = 0$ and $dV/dz = \sigma$ as $z \to \infty$. Here η is the ratio of the segment's friction coefficient to that of a Stokes sphere with diameter l, and $f(\varphi)$ is a function that accounts for hydrodynamic interactions among segments. Without hydrodynamic interaction, $f = 1$; following Cohen Stuart et al.,[10] we employ $f = 1/(1 - \xi\varphi)$, as suggested by experimental data,[28] where ξ is the fraction of a segment volume actually occupied by polymer (see eq 56).

After $dV/dz|_{z=0}$ is guessed, eq 51 is integrated numerically as a system of two simultaneous first-order equations. The integration continues until a point $z = z_L$ where the shear rate σ is constant. The hydrodynamic thickness, given by

$$t_H = z_L - \frac{V(z_L)}{\sigma} \tag{52}$$

is the apparent position of a hypothetical "clean" surface that would give a linear velocity profile with the same shear rate (see Figure 2); t_H is independent of shear rate.

Results and Discussion

A. Determination of Model Parameters. Comparison of theoretical predictions with experimental data is instructive, providing the means of testing the assumptions of this model. First, though, the experimental system's physical characteristics must be translated into the model parameters; these conversion factors deserve some explanation.

The necessary physical parameters are the polymer's characteristic ratio, molecular weight, average bond length, and specific volume, denoted by C_∞, M, l_b, and $\bar{v}$, respectively, and polymer–solvent parameters including the entropy parameter, ψ_1, and the Θ temperature. There are little data for segment–surface interaction energies, so χ_s

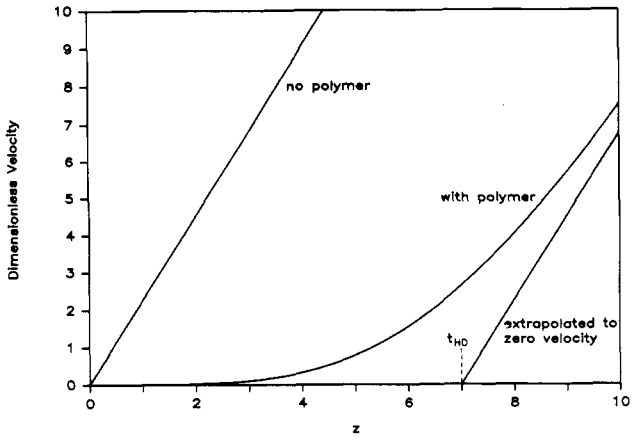

Figure 2. Solvent velocity profiles for imposed shear flow past a planar surface. Extrapolation of the profile for flow through a polymer layer back to zero velocity, parallel to the profile found when no polymer is adsorbed, gives the hydrodynamic thickness of the layer.

is left as an adjustable parameter. Denoting $\langle r^2\rangle_0$ as the mean-squared end-to-end distance and r_{max} as the maximum extended length of a freely jointed chain, the relations

$$\langle r^2\rangle_0 = C_\infty n_b l_b^2 \equiv nl^2 \tag{53a}$$

$$r_{max} = n_b l_b \equiv nl \tag{53b}$$

can be solved for n and l in terms of l_b and $n_b \equiv M/m_b$, where m_b is the polymer molecular weight per bond. Thus

$$l = C_\infty l_b \tag{54}$$

and

$$n = M/C_\infty m_b \tag{55}$$

Segments have volume but are not solid polymer. If segments are assumed to be spherical,

$$\xi = \frac{6\tilde{v}C_\infty m_b}{\pi l^3 N_A} \tag{56}$$

is the fraction of a segment volume occupied by polymer, where N_A is Avogadro's number. If c_b is the polymer concentration in bulk solution (mass per volume) and A is the polymer adsorbance (adsorbed mass per area of surface), the corresponding theoretical quantities are

$$\varphi_b = c_b\tilde{v}/\xi \tag{57}$$

and

$$\varphi_{ads} = A\tilde{v}/C_\infty l_b \tag{58}$$

Finally, the definition[23]

$$\chi = \frac{1}{2} - \psi_1\left(1 - \frac{\Theta}{T}\right) \tag{59}$$

gives the solvent quality parameter as a function of temperature.

B. Volume Fraction Profiles of Polymer Segments. Representative volume fraction profiles are shown in Figure 3, with volume fraction scaled logarithmically. The profile found from the ground-state solution decays linearly, indicating that the exponential in the numerator of eq 46 dominates. We have also calculated the volume fraction profile from the lattice model equations of Scheutjens and Fleer.[8] This profile (also in Figure 3) decays more slowly and nonlinearly; the points mark the discrete layers for which the volume fraction is given by this model. A straightforward calculation produces subsidiary profiles of the volume fractions of segments contained in loop and tail configurations. The region near the wall is depleted of tail segments, and the tail segment profile has a slight maximum reminiscent of the profiles of terminally anchored chains. Farther from the surface, the loop segment profile falls off linearly as the total profile becomes dominated by tails.

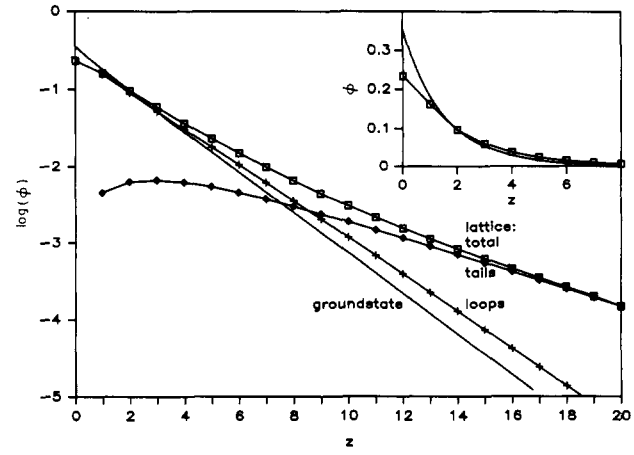

Figure 3. Polymer volume fraction profiles predicted by the ground-state and lattice models, plotted on a logarithmic scale. The discrete layers of the lattice model at which the volume fractions are known are marked with symbols. The total polymer volume fraction profiles of the lattice and ground-state profiles are plotted on a linear scale in the inset. The lattice model predictions for the volume fraction profiles of segments contained in loops and tails are also shown. The parameters are $n = 10^3$, $\varphi_b = 10^{-6}$, $\chi_s = 0.25$, $\chi = 0.5$, $\xi = 1$; the lattice parameter is $\lambda = {}^1/_6$.

The similarity between the ground state and loop profiles is significant, suggesting that the ground-state model predicts an adsorbed layer primarily composed of loops. Transformation of the SCF equation (26) to the form (37) via the ground-state approximation (35) eliminates the dependence of the configuration probability, $G_c(z,s)$, and volume fraction of particular segments, $\varphi_c(z,s)$, on contour location s. Consequently, within the ground-state approximation, the position of a segment relative to the surface *does not* depend on the segment's location or rank within the chain. Thus, "end" segments and tails are not predicted; all segments are "middle" segments contained in loops or trains. The same result is found in the analysis of eigenfunction expansion solutions by Scheutjens et al.[40]

More quantitative comparisons with the lattice model are difficult for two reasons. First, the lattice calculation relies on an adjustable lattice parameter, λ, which dramatically affects the shape of the profile and the adsorbed amount. Our lattice calculations employ a value of $\lambda = {}^1/_6$ (simple cubic), chosen to match the "diffusivity" of the configuration probability with that in the ground-state model. Second, although the ground-state and lattice models give solutions of the same field equation, the surface boundary conditions are different. The lattice model employs the classic "adsorption" boundary condition; that is, there are no segments at positions one segment length behind the surface surface. The boundary condition developed here includes the "sticky surface" adsorption leading to a mixed boundary condition and producing a source of configuration probability at the surface due to adsorbed segments. Although the two approaches do not necessarily lead to the same adsorbed amount, the predicted values of φ_{ads} are comparable (0.658 and 0.563 from the lattice and ground-state models, respectively, for the conditions in Figure 3).

C. Adsorption Isotherms. Qualitatively, the adsorption isotherms of the ground-state model, depicted in

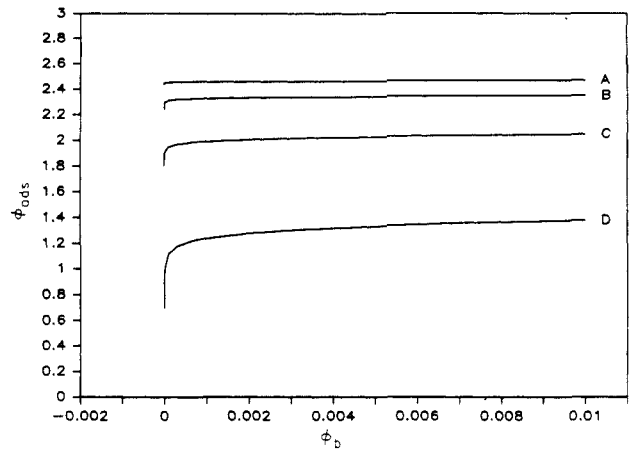

Figure 4. Adsorption isotherms (φ_{ads} versus φ_b) from the present model for several chain lengths: curves A–D are for $n = 10^6$, 10^5, 10^4, and 10^3, respectively. Also $\chi_s = 0.25$, $\chi = 0.45$, and $\xi = 1$.

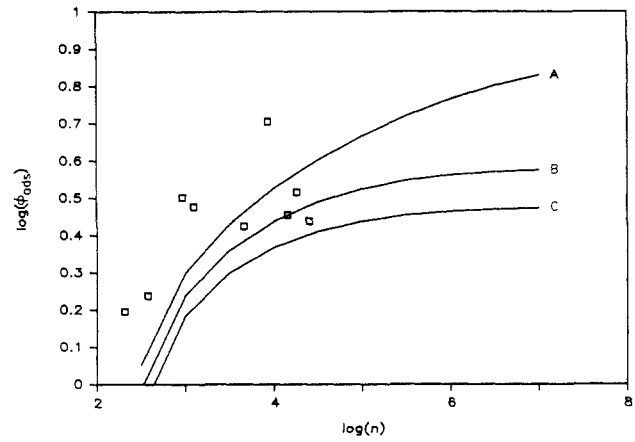

Figure 5. Adsorbed amount versus chain length: the points are the ellipsometric data of Takahashi et al.[32] for adsorption of polystyrene on chrome in cyclohexane at the Θ point; the curves are the ground-state model predictions at near-Θ and good-solvent conditions with $\chi = 0.4993$, 0.4824, and 0.4660 for curves A, B, and C, respectively. Also $\chi_s = 0.25$, $\varphi_b = 6.91 \times 10^{-3}$, and $\xi = 0.4027$.

Figure 4, closely resemble the experimental isotherms found through ellipsometry.[30-35] As φ_b increases from 10^{-9}, the equilibrium adsorbed amount rapidly reaches a plateau value that increases with chain length. An informative comparison with experiment, Figure 5, shows the adsorbed amount as a function of chain length on a log–log scale. The points are the experimental data of Takahashi et al.[32] for polystyrene adsorbing on chrome from cyclohexane at the Θ temperature; the curves are the ground-state model predictions. The value $\chi_s = 0.25$ is selected so that the ground-state curve for $\chi = 0.4993$ passes roughly through the data. Values in the range $0.10 < \chi_s < 0.50$ fit individual points, but no curve passes through all or most of the data. The adsorbed amount increases with chain length, agreeing with all ellipsometric data. For adsorption from a Θ solvent, Takahashi et al.[32] suggest that φ_{ads} definitely levels off at moderate chain lengths, despite considerable scatter in the data. The ellipsometric data of Killmann et al.[33] and the infrared data of vander Linden and van Leemput[36] (for polystyrene adsorption on amorphous silica from cyclohexane) show no plateau, or at least a more gradual transition, although they may not have used sufficiently long chains. The ground-state curve exhibits decreasing slope but does not quite reach a plateau.

Competition between segment–surface attraction and the net repulsion between segments explains these trends.

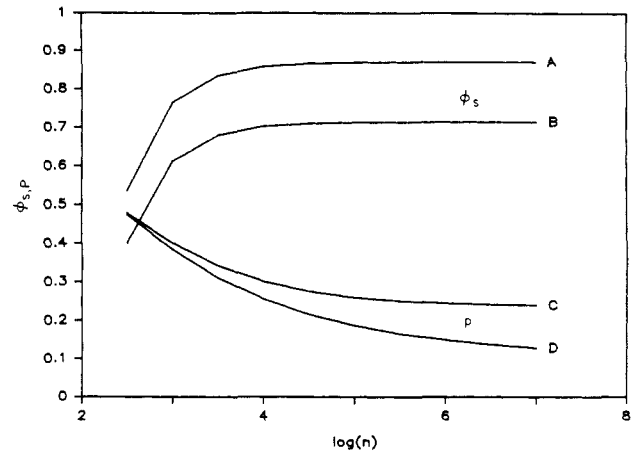

Figure 6. Ground-state model predictions for the surface volume fraction and bound fraction versus chain length. For curves A and D, $\chi = 0.4993$; for curves B and C, $\chi = 0.4660$. Also $\chi_s = 0.25$, $\varphi_b = 6.91 \times 10^{-3}$, and $\xi = 0.4027$.

Surface attraction (adsorption) draws chains into the adsorbed layer and tends to bring segments together at all spatial points. Chains adsorb until the decrease in free energy due to segment adsorption is balanced by the loss of chain configurational entropy. Since longer chains lose a smaller fraction of their configurational entropy upon adsorption, the adsorbed amount increases with chain length.

Adsorption is also opposed by segment–segment repulsion which increases the free energy. The net interaction between segments, represented by

$$1 - e^{\beta U_c} \approx -\upsilon\varphi_c - \frac{w}{2}\varphi_c^2 \qquad (60)$$

drives the SCF equation (37). The "excluded volume" $\upsilon = \xi(1 - 2\chi)$ contains entropic repulsion due to volume exclusion between segments (1) mediated by the segment–solvent attraction (-2χ); the sum is multiplied by ξ to account for the volume of segments not occupied by polymer. In a Θ solvent, $\upsilon = 0$, and the interaction is a weak repulsion due to the $\mathcal{O}(\varphi_c^2)$ term in (60). In this case the surface attraction usually dominates the repulsion so that φ_{ads} increases consideraly with n (Figure 5). In "good" solvents ($\upsilon > 0$), the $\mathcal{O}(\varphi_c)$ repulsion contributes significantly to the free energy, enough to counter the energy loss due to segment adsorption and limit the volume fraction at all spatial points, independent of chain length. As chain length increases, the layer reaches its capacity when the attraction balances the repulsion so that the adsorbed amound levels off. Improvement in solvent quality (υ increases or χ decreases) heightens the segment–segment repulsion and reduces the adsorbed amount.

D. Surface Volume Fraction and Bound Fraction. The explanations for the trends in the adsorbed amount are also supported by calculations indicative of chain structure. The bound fraction, p, and the surface volume fraction, φ_s, are shown as functions of chain length in Figure 6. The surface volume fraction reaches a limiting value at moderate chain lengths when the free energy loss due to segment adsorption is balanced by their mutual repulsion at the surface; φ_s is less in a good solvent since the repulsion is greater than in a Θ solvent. The bound fraction, i.e., the fraction of segments adsorbed on the surface, decreases with increasing chain length, indicating that longer chains are adsorbed in more extended configurations. This prediction agrees well with the experimental data of vandar Linden and van Leemput.[36] Fewer chains adsorb from a good solvent than from a Θ solvent, but if

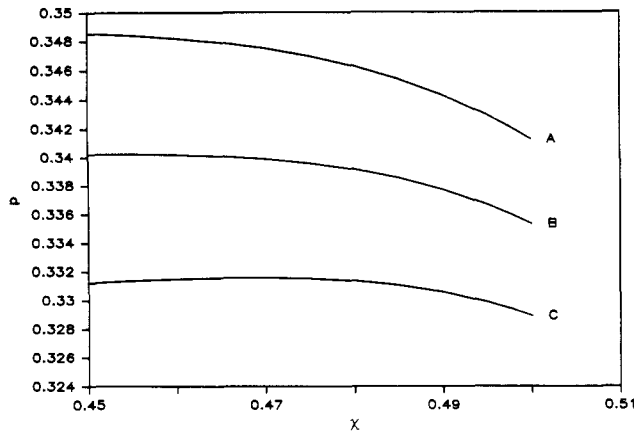

Figure 7. Bound fraction versus solvent quality parameter for three adsorption strengths, calculated from the ground-state model. Curves A, B, and C are for χ_s = 0.16, 0.15, and 0.14, respectively. Also $n = 10^3$, $\varphi_b = 6.91 \times 10^{-3}$, and $\chi = 0.4027$.

the adsorption strength is high, the adsorbing chains assume flatter configurations (seen in the higher bound fraction).

A clearer picture of this effect is furnished by the results in Figure 7 showing the bound fraction as a function of the solvent quality parameter, χ, for three adsorption strengths, χ_s. At the highest adsorption strength, increasing solvent quality (decreasing χ) produces flatter configurations, as indicated by the higher bound fraction. The number of adsorbed chains and the volume fraction at all points decrease faster than the excluded volume increases, giving an overall reduction in segment–segment repulsion; thus adsorption has a greater influence on the chains, leading to flatter configurations. At lower values of χ_s, though, fewer chains are already adsorbed; as χ decreases, the net repulsion between segments eventually increases since the excluded volume grows faster than the volume fraction falls. Consequently, adsorbing chains have a lower bound fraction and more extended configurations.

E. Root-Mean-Square Layer Thickness. Another important characteristic of polymer adsorption is the layer thickness. The ellipsometric thickness is proportional[30] to the root-mean-square (RMS) thickness defined in eq 50. Figure 8 shows the variation of t_{RMS} with n, as measured by Takahashi et al.[32] for adsorption from a Θ solvent and as predicted by the ground-state model. The calculated thickness is much less than the experimental thickness, presumably due to the underestimation of tails by the ground-state model. Although the volume fraction of segments far from the surface is relatively low, they probably make a significant contribution to t_{RMS} due to the z^2 factor in the integrand of (50). The lattice model result of Figure 3 indicates that the distant segments are found primarily in tail configurations.

The power law dependence of t_{RMS} on n is also significant. Ellipsometric data,[30-33,35] lattice model predictions,[8] and a scaling theory analysis[34] find that $t_{RMS} \approx n^{0.5}$ in a Θ solvent, suggesting that chains adsorb as random coils. The smaller exponent, 0.415, calculated from the present model is consistent with the scaling of t_{RMS} expected for chains adsorbed in loops and trains but not tails. The data and scaling analysis of Kawaguchi and Takahashi[34] gives $t_{RMS} \approx n^{0.4}$ in good solvents. As before, the calculated exponent, 0.279, is less than the experimental value, but it is also less than the calculated Θ solvent exponent.

Other ellipsometric data[32] clearly show that the RMS thickness is greater for adsorption from a good solvent than a Θ solvent, but the predictions of the ground-state and lattice models are just the opposite for these conditions.

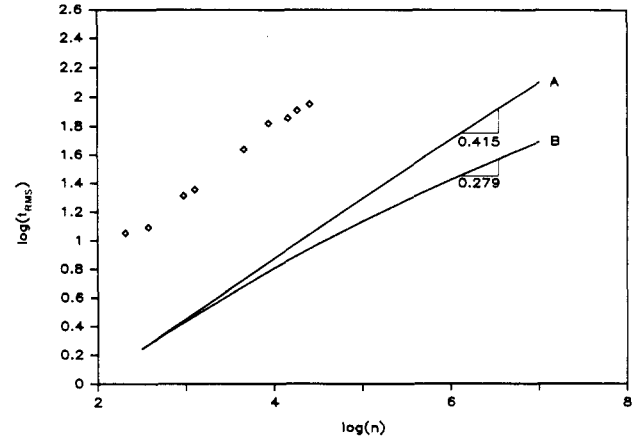

Figure 8. Root-mean-square thickness versus chain length from the ellipsometric data of Takahashi et al.[32] for adsorption from a Θ solvent (points), and the ground-state model predictions for a Θ and a good solvent with χ = 0.4993 and 0.4660 for curves A and B. Also χ_s = 0.25, $\varphi_b = 6.91 \times 10^{-3}$, and ξ = 0.4027.

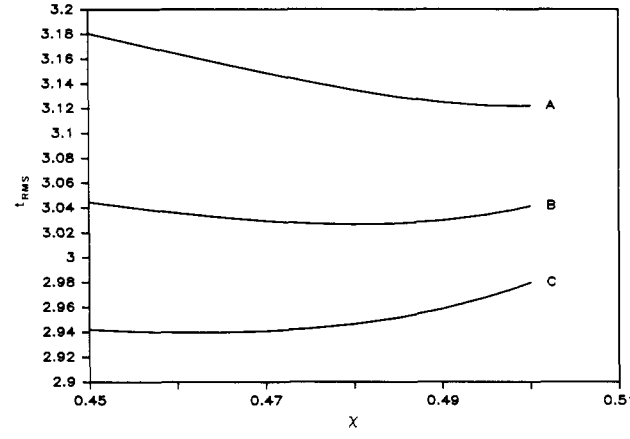

Figure 9. Ground-state model results for root-mean-square thickness versus solvent quality parameter for three adsorption strengths: χ_s = 0.14, 0.16, and 0.18 for curves A, B, and C, respectively. Also $n = 10^3$, $\varphi_b = 6.91 \times 10^{-3}$, and ξ = 0.4027.

Again, the balance between segment adsorption and their mutual repulsion explains the results. The variation of RMS thickness with solvent quality for three adsorption strengths is given in Figure 9. Decreasing χ improves the solvent quality and allows fewer chains to adsorb. For the same reasons cited in the discussion of Figure 7, improvement of solvent quality at high adsorption strength leads to flatter configurations and a lower RMS thickness. The reduced number of segments on the surface experience greater mutual repulsion that is balanced through adsorption of a larger fraction of the segments. At low adsorption strength or in a very good solvent, the product of excluded-volume and surface-volume fraction increases with χ (although φ_s decreases); the greater repulsion produces more extended configurations and greater RMS thickness.

F. Hydrodynamic Layer Thickness. Hydrodynamic methods provide another measure of layer thickness. Given a volume fraction profile such as provided by eq 46, integration of the Debye–Brinkmann equation (51) yields the solvent velocity profile; extrapolation from the limit of constant shear back to zero velocity gives the hydrodynamic (HD) thickness, t_{HD}, as illustrated in Figure 2. The dependence of t_{HD} on n, shown in Figure 10, includes the experimental data of Cohen Stuart et al.[10] for poly(ethylene oxide) adsorbing on polystyrene particles suspended in water, with t_{HD} measured through dynamic light scattering. The groundstate model predicts HD thick-

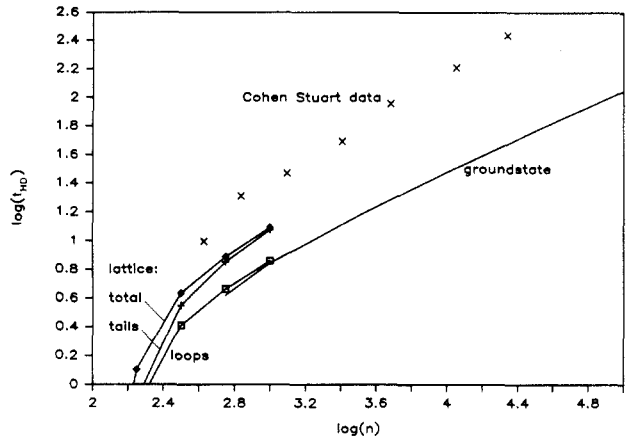

Figure 10. Hydrodynamic thickness versus chain length: the points are the data of Cohen Stuart et al.[10] for adsorption of poly(ethylene oxide) on silica in water, measured through dynamic light scattering; also shown are the thicknesses derived from volume fraction profiles given by the ground-state model and the lattice model (including the individual contributions of loops and tails). Parameters include $\varphi_b = 4.1 \times 10^{-4}$, $\chi_s = 0.25$, $\chi = 0.45$, $\xi = 0.7109$, $\eta = 1.0$, and $\lambda = {}^1/_6$.

nesses (with $\eta = 1$) considerably smaller than the experimental values. As with the RMS thickness, this discrepancy is attributed to the lack of tails inherent in the ground-state solution of the SCF equations. Following Cohen Stuart et al.,[10] we compute t_{HD} utilizing the volume fraction profiles for segments in loops, tails, and the total profile furnished by the lattice model. The HD thickness due to loops is comparable to that of the ground-state model, consistent with our conclusion that the ground-state solution predicts only loop–train configurations. The thicknesses derived from the tail segment and total profiles are almost the same and are, perhaps coincidentally, close to the experimental values. The former observation supports the contention of Cohen Stuart et al.[10] and Anderson and Kim[27] that tails dominate the hydrodynamic behavior of adsorbed polymer layers.

Conclusions

The derivation of the SCF equations (26)–(33) is based on three assumptions: that the real polymer molecule can be modeled as a chain of statistical segments, that the probability of a chain configuration is the product of individual segment Boltzmann factors and bond probabilities, and that the chain statistics represent a Markov process. Notwithstanding the specification of the self-consistent field (determining the functional form of all segment interactions), the continuous space formalism developed here should be considered a general model. The potential field itself is more than just a mean field: it is a *self-consistent* mean field, similar to a potential of mean force, that recognizes the influence of other segments and solvent molecules in the local environment, if not explicit correlations among segments. Helfand's definition of the self-consistent field, derived through statistical mechanics from the total partition function of the system, ensures that an equilibrium distribution of chain configurations appears in the absorbed layer.

This continuous space approach improves upon earlier models in two ways. First, the model is independent of lattice parameters, eliminating the rationalization of lattice geometry based on presumed chain structure. However, the present formulation introduces spatial anisotropy within one segment length of the surface. We do not address this problem, believing that it is really subsumed by the problem of understanding the true form of the polymer–surface interaction. A second advantage of this model is its versatility in the specification of all segment interactions through incorporation of an arbitrary polymer solution theory, an advantage largely due to the generality of Helfand's equations. Of course, the polymer adsorption model necessarily suffers any shortcomings of the polymer solution theory.

Recent simulations and theoretical analyses[19] suggest that the Flory solution theory, developed for chains on a lattice, seriously underestimates segment–segment repulsion relative to continuous space calculations. Such an error may explain some of the quantitative discrepancies between experimental data and the ground-state model predictions. If the coefficients v and w in eq 60 are considerably larger in a proper continuous space formulation, the segment–segment repulsion becomes more important, especially for shorter chains, at lower volume fractions, and at higher adsorption strengths. Greater repulsion should, for example, produce lower plateaus in the adsorbed amount as chain length increases, and the plateau should begin at lower chain lengths.

Other predictions currently give qualitative but not quantitative agreement with experiment. The calculated RMS thickness, in Figure 8, is less in a good solvent than in a Θ solvent, a prediction that is just the opposite of the experimental observation. However, the results in Figure 9 identify regions in the parameter space of the model that lead to qualitatively correct predictions. Greater repulsion between segments would shift such behavior to longer chains and higher adsorption strengths. An important problem, then, is the development of more accurate expressions for the interactions between segments and with the surface, leading to better quantitative agreement between theory and experiment.

Drastic approximations are made in the solution of the general SCF equations. The numerical solution obtained through the lattice model gives detailed configurational statistics but introduces the artificiality of the lattice; this solution also has computational limitations and obscures some of the physical aspects of the problem. The ground-state solution produces analytical results and begins to clarify the physical picture, but the neglect of segment rank in the solution precludes the analysis of specific chain configurations and the prediction of tails. The model's ignorance of tails causes underestimation of both the root-mean-square and hydrodynamic thicknesses.

Although the predictive power of the ground-state model is rather limited, this self-consistent scheme presents several interesting opportunities for development. The ground-state solution (46) could be used to generate an approximate self-consistent field that can be employed in a more sophisticated numerical solution of the general equation (26). A simpler method relies on the observation that far from the surface, chain configurations are not significantly perturbed from the Gaussian random-walk state. A matching procedure could generate a uniformly valid approximate solution that reduces to the ground-state solution close to the surface, where the chains are grossly distorted by adsorption, and passes smoothly to the properties of the bulk solution far from the surface. Such an analysis will provide a more complete description of configurational statistics, especially tails. As mentioned earlier, an improved polymer solution theory, such as the generalized Flory or Flory–Huggins theory,[19] may give a better estimate of segment–segment interactions in continuous space. Incorporation of more accurate energy expressions into the general model for homopolymer adsorption, combined with more advanced solution tech-

niques, should improve quantitative comparison with experimental results and provide a better understanding of this and other polymer-modified interfacial systems.

Acknowledgment. We gratefully acknowledge the support of the Chemical Sector of the Allied Corporation.

Registry No. Cr, 7440-47-3; Si, 7631-86-9; polystyrene, 9003-53-6; poly(ethylene oxide), 25322-68-3.

References and Notes

(1) Napper, D. H. *Polymeric Stabilization of Colloidal Dispersions*; Academic: New York, 1983. Sato, T.; Ruch, R. *Stabilization of Colloidal Dispersions by Polymer Adsorption*; Marcel Dekker: New York, 1980.
(2) Stromberg, R. R. In *Treatise on Adhesion and Adhesives*; Patrick, R. J., Ed.; Marcel Dekker: New York, 1967; p 69. Lipatov, Yu. S.; Sergeeva, L. M. *Adsorption of Polymers*; Wiley: New York, 1974. Vincent, B. *Adv. Colloid Interface Sci.* **1974**, *4*, 93. Eirich, F. *J. Colloid Interface Sci.* **1977**, *58*, 423. Vincent, B.; Whittington, S. G. *Surf. Colloid Sci.* **1982**, *12*, 1. Molyneux, P. *Water-Soluble Synthetic Polymers: Properties and Behavior*; CRC Press: Boca Raton, FL, 1982; Vol. 2, Chapter 4. Takahashi, A.; Kawaguchi, M. *Adv. Polym. Sci.* **1982**, *46*, 1. Tadros, Th. F. In *The Effect of Polymers on Dispersion Properties*; Tadros, Th. F., Ed.; Academic: New York, 1982; p 1. Fleer, G. J.; Lyklema, J. In *Adsorption from Solution at the Solid/Liquid Interface*; Parfitt, G. D., Rochester, C. H., Eds.; Academic: New York, 1983; p 153.
(3) Frisch, H. L.; Simha, R.; Eirich, F. R. *J. Chem. Phys.* **1953**, *21*, 365. DiMarzio, E. A. *J. Chem. Phys.* **1965**, *42*, 2101. Rubin, R. J. *J. Chem. Phys.* **1965**, *43*, 2392. Roe, R. J. *J. Chem. Phys.* **1965**, *43*, 1591. Silberberg, A. *J. Chem. Phys.* **1966**, *46*, 1105.
(4) Chan, D.; Mitchell, D. J.; Ninham, B. W.; White, L. R. *J. Chem. Soc., Faraday Trans. 2* 1975, *71*, 235.
(5) Silberberg, A. *J. Chem. Phys.* **1967**, *48*, 2835. Hoeve, C. A. J. *J. Polym. Sci., Part C* **1970**, *30*, 361; **1971**, *34*, 1.
(6) McCrackin, F. L. *J. Chem. Phys.* **1967**, *47*, 1980. Clark, A. T.; Lal, M.; Turpin, M. A.; Richardson, K. A. *Faraday Discuss. Chem. Soc.* **1975**, *59*, 189. Lal, M.; Stepto, R. F. T. *J. Polym. Sci., Polym. Lett. Ed.* **1977**, *61*, 401.
(7) Roe, R. J. *J. Chem. Phys.* **1973**, *60*, 4192. Helfand, E. *Macromolecules* **1975**, *9*, 307. Levine, S.; Thomlinson, M. M.; Robinson, K. *Faraday Discuss. Chem. Soc.* **1978**, *65*, 202.
(8) Scheutjens, J. M. H. M.; Fleer, G. J. *J. Phys. Chem.* **1979**, *83*, 1619; **1980**, *84*, 178. Scheutjens, J. M. H. M.; Fleer, G. J. *Macromolecules* **1985**, *18*, 1882.
(9) Chandrasekhar, S. *Rev. Mod. Phys.* **1943**, *15*, 1. Hesselink, F. Th. *J. Phys. Chem.* **1973**, *73*, 3488; **1971**, *75*, 65.
(10) Cohen Stuart, M. A.; Waajen, F. H. F. H.; Cosgrove, T.; Vincent, B.; Crowley, T. L. *Macromolecules* **1984**, *17*, 1825.
(11) Klein, J. *J. Chem. Soc., Faraday Trans. 1* **1983**, *79*, 99. Klein, J.; Luckham, P. *Macromolecules* **1984**, *17*, 1041. Klein, J. *J. Colloid Interface Sci.* **1986**, *111*, 305.
(12) Edwards, S. F. *Proc. Phys. Soc.* **1965**, *85*, 613.
(13) de Gennes, P.-G. *Rep. Prog. Phys.* **1969**, *32*, 187.
(14) Jones, I. S.; Richmond, P. *J. Chem. Soc., Faraday Trans. 2* **1977**, *73*, 1062.
(15) de Gennes, P.-G. *Scaling Concepts in Polymer Physics*; Cornell University Press: Ithaca, NY, 1979.
(16) van Kampen, N. G. *Stochastic Processes in Physics and Chemistry*; North-Holland: New York, 1985.
(17) Freed, K. F. *Adv. Chem. Phys.* **1972**, *22*, 1.
(18) Helfand, E. *J. Chem. Phys.* **1975**, *62*, 999. Helfand, E.; Sapse, A. M. *J. Chem. Phys.* **1975**, *62*, 1327. Helfand, E.; Sapse, A. M. *J. Polym. Sci., Polym. Symp.* **1976**, *54*, 289.
(19) Dickman, R.; Hall, C. K. *J. Chem. Phys.* **1986**, *85*, 4108.
(20) Baxter, R. J. *J. Chem. Phys.* **1969**, *49*, 2770.
(21) Helfand, E. *Macromolecules* **1975**, *8*, 552. Helfand, E.; Wasserman, Z. R. *Macromolecules* **1976**, *9*, 879.
(22) Flory, P. J. *Principles of Polymer Chemistry*; Cornell University Press: Ithaca, NY, 1953.
(23) Joanny, J. F.; Leibler, L.; de Gennes, P.-G. *J. Polym. Sci., Polym. Phys. Ed.* **1979**, *17*, 1073.
(24) Barnett, K.; Cosgrove, T.; Crowley, T. L.; Tadros, Th. F.; Vincent, B. In *The Effect of Polymers on Dispersion Properties*; Tadros, Th. F., Ed.; Academic: London, 1982; p 183.
(25) Cosgrove, T.; Vincent, B.; Crowley, T. L.; Cohen Stuart, M. A. *ACS Symp. Ser.* **1984**, *240*, 147.
(26) Varoqui, R.; Dejardin, P. *J. Chem. Phys.* **1977**, *66*, 4395.
(27) Anderson, J. L.; Kim, J. O. *J. Chem. Phys.* **1987**, *86*, 5163.
(28) Mijnlieff, P. F.; Jaspers, W. J. *Trans. Faraday Soc.* **1971**, *67*, 1837. Vidakovic, P.; Allain, C.; Rondelez, F. *Macromolecules* **1982**, *15*, 1571.
(29) Dolan, A. K.; Edwards, S. F. *Proc. R. Soc. London A* **1974**, *337*, 509; **1975**, *343*, 427.
(30) Stromberg, R. R.; Passaglia, E.; Tutas, D. J. *J. Res. Natl. Bur. Stand., Sect. A* **1963**, *67*, 431. Stromberg, R. R.; Passaglia, E.; Tutas, D. J. *J. Phys. Chem.* **1965**, *69*, 3955.
(31) Kawaguchi, M.; Hayakawa, K.; Hirota, H.; Kato, T. *Macromolecules* **1980**, *13*, 884.
(32) Kawaguchi, M.; Takahashi, A. *J. Polym. Sci., Polym. Phys. Ed.* **1980**, *18*, 2069. Killmann, E.; Wiegand, H.-G. *Makromol. Chem.* **1970**, *132*, 239.
(33) Killmann, E.; Eisenlauer, J.; Korn, M. *J. Polym. Sci., Polym. Symp.* **1977**, *61*, 413.
(34) Kawaguchi, M.; Hayakawa, K.; Takahashi, A. *Macromolecules* **1983**, *16*, 631. Kawaguchi, M.; Takahashi, A. *Macromolecules* **1983**, *16*, 1465.
(35) Killmann, E.; von Kuzenko, M. *Angew. Makromol. Chem.* **1974**, *35*, 39.
(36) vander Linden, C.; van Leemput, R. *J. Colloid Interface Sci.* **1978**, *67*, 48.
(37) Fontana, B. J.; Thomas, R. J. *J. Phys. Chem.* **1961**, *65*, 480. Thies, C. *J. Phys. Chem.* **1966**, *70*, 3783. Thies, C. *J. Polym. Sci., Part C* **1971**, *34*, 201. Herd, J. M.; Hopkins, A. J.; Howard, G. J. *J. Polym. Sci., Part C* **1971**, *34*, 211. Day, J. C.; Robb, I. D. *Polymer* **1980**, *21*, 408.
(38) Barnett, K. G.; Cosgrove, T.; Vincent, B.; Sissons, D. S.; Cohen Stuart, M. A. *Macromolecules* **1981**, *14*, 1018. Cosgrove, T.; Barnett, K. *J. Magn. Reson.* **1983**, *43*, 15. Miyamoto, T.; Cantow, H.-J. *Makromol. Chem.* **1972**, *162*, 43.
(39) Robb, I. D.; Smith, R. *Polymer* **1977**, *18*, 500.
(40) Scheutjens, J. M. H. M.; Fleer, G. J.; Cohen Stuart, M. A. *Colloids Surf.* **1986**, *21*, 285.
(41) Ploehn, H. J. Ph.D. Thesis, Princeton University, Princeton NJ, 1988.